Cement and Concrete Research 134 (2020) 106078

Contents lists available at ScienceDirect

Cement and Concrete Research

journal homepage: www.elsevier.com/locate/cemconres

Influence of process parameters on the interlayer bond strength of concrete elements additive manufactured by Shotcrete 3D Printing (SC3DP)

Harald Kloft[a,*], Hans-Werner Krauss[b], Norman Hack[a], Eric Herrmann[a], Stefan Neudecker[c], Patrick A. Varady[b], Dirk Lowke[b]

[a] Technische Universität Braunschweig, Institute of Structural Design (ITE), Pockelsstr. 4, 38106 Braunschweig, Germany
[b] Technische Universität Braunschweig, Institute of Building Materials, Concrete Construction and Fire Safety (iBMB), Beethovenstr. 52, 38106 Braunschweig, Germany
[c] Folkwang University of the Arts Essen, Design by Technology, Martin-Kremmer-Str. 21, 45327 Essen, Germany

ARTICLE INFO

Keywords:
Shotcrete 3D Printing
SC3DP
Additive Manufacturing
Cold joints
Interlayer bond strength

ABSTRACT

Shotcrete 3D Printing (SC3DP) is a novel robot-guided AM technology developed at Technische Universität Braunschweig in the environment of the Digital Building Fabrication Laboratory (DBFL). For successful automation, it is crucial to understand and redefine the entire concrete spraying process with all its interdependent parameters. This paper presents the basic principles of the SC3DP technology together with the results of a comparative study on the influence of the two concrete printing techniques extrusion and SC3DP on the interlayer bond strength. In particular, the effect of different time intervals between the deposition of two adjacent layers regarding mechanical properties (bond strength) is investigated. As will be shown, the SC3DP method allows convenient mechanical properties although the printed samples exhibit distinct anisotropies. The reasons are discussed based on investigations of the air void distribution by micro CT and mechanical test results.

1. Introduction

Today, many industrial sectors use Additive Manufacturing (AM) for production of individualized and geometrically complex parts and products [1]. Originally, AM was used for the rapid production of prototypical workpieces (rapid prototyping), aiming at fast verification cycles for design and function. The basic principles of Additive Manufacturing are ideally suited for individualized production in the construction industry, as more or less every building is subject to a prototypical manufacturing approach due to the different local conditions. Thus, Additive Manufacturing in construction will offer designers and construction industry several advantages, such as higher productivity, less geometric design limitations, customized design and production, improved process quality control, as well as integrative design of different functions. Moreover, AM in construction will contribute to an efficient use of resources, an increased quality and an improved safety during the construction process [2,3]. However, there are specific challenges for a successful transfer of AM to the construction industry: firstly, the large scale of the components and structures, and secondly, the transformation of the predominantly manual manufacturing techniques into fully automated digital processes.

For layered component construction, the design geometry is sliced in two-dimensional layers and then converted into path planning data. Since no formwork is used, the production process relies on self-supporting of the material, i.e., the existing material layers have to bear the load of the following layers. The most widespread method of AM in concrete construction is extrusion 3D printing [4]. In contrast to cast concrete elements, 3D printed concrete elements exhibit pronounced anisotropic material properties due to the layer-by-layer deposition. This may result in weaker bonds between two adjacent layers, so called “cold joints”, depending on the individual material and process parameters [5,6]. Hence, one of the key issues to ensure the demanded mechanical and durability performance is to ensure proper interlayer bond strength. Interlayer bond strength depends on numerous influencing factors such as viscosity, yield stress and thixotropy of the printed material, pumping pressure, pumping distance, printing speed, nozzle shape, etc. One decisive influencing factor on the risk of cold joint formation is the delay time between the deposition of two subsequent layers [5]. Depending on the actual material composition, rheological properties and fabrication velocity, the critical timeframe (delay time) may vary within a broad range. Although several experimental studies on the anisotropies and bond properties of extruded 3D printed concrete have been published, see e.g. [7–18], the problem of cold joint formation is still a largely open field of research [19].

* Corresponding author.
E-mail address: h.kloft@tu-braunschweig.de (H. Kloft).

https://doi.org/10.1016/j.cemconres.2020.106078
Received 19 December 2019; Received in revised form 18 March 2020; Accepted 8 April 2020
Available online 11 May 2020
0008-8846/

However, existing knowledge on adhesion mechanisms between old concrete and concrete repair may be applicable [11].

Generally, bond strength between concrete layers is largely determined by adhesion mechanisms, which can be differentiated into mechanical interaction, chemical bonding and thermodynamic mechanisms [20]. It was found that a higher roughness of the interface between the old and new concrete layer was less susceptible to ageing of bond properties, i.e., loss of bond strength, and that micro-crack formation (due to surface preparation, shrinkage or other effects) is a main reason for ageing [21]. The positive effect of interlocking (i.e., macroscopic roughness) on interface bond strength of layered specimens was confirmed e.g. by [12]. The effect was more pronounced for splitting tensile strength than for compressive strength, which indicates that the increase in bond strength could partially be due to the increase in contact surface of the layers [12], which was confirmed by [16,22]. Moreover, interlayer adhesion is influenced by the mix composition (water-to-cement ratio, binder composition, aggregates, etc.), the amounts of pores, voids, and micro-cracks at the interface as well as the delay time between the deposition of two subsequent layers [8,9,22]. For a more detailed summary of the state-of-the-art on the influencing factors and mechanisms of interlayer mechanical properties see e.g. [9,23].

This paper presents investigations on interlayer bond strength of the so-called Shotcrete 3D Printing (SC3DP) technology. SC3DP is an automated robotic AM technology developed in an interdisciplinary joint project at Technische Universität Braunschweig [24–28]. The SC3DP technique is based on material spraying, with concrete components being built up layer-by-layer. The material is accelerated at the nozzle by controlled addition of compressed air. The high kinetic energy of the material results in proper compaction of the concrete layers and good mechanical bond between two successive layers [27,29]. In this paper, the basic working principles of the SC3DP technology and the corresponding robotic workspace “Digital Building Fabrication Laboratory” (DBFL) at TU Braunschweig are presented first. Subsequently, the potentials and capabilities of SC3DP are demonstrated by means of experimental studies on the mechanical and structural properties as compared to extruded test specimens. As will be shown, layer interlocking, and hence, interlayer bond strength, are enhanced due to the high kinetic energy of the sprayed material, which helps mitigating the risk of cold joints formation.

2. The Shotcrete 3D Printing (SC3DP) technology

2.1. Digital Building Fabrication Laboratory (DBFL)

The Digital Building Fabrication Laboratory (DBFL) provides the robot-guided manufacturing environment of the SC3DP technology. The DBFL consists of two independent digital fabrication units, each attached to a separate rigid portal in an enclosed building area, which can perform processes synchronously, cooperatively or independently. Each portal can position itself in the cooperative working space of 2.50 m × 5.24 m × 10.52 m (height x width x length) with an accuracy of 0.5 mm. The maximum gantry speed is 44 m/min for the x- and y-axis and 20 m/min for the z-axis (Fig. 1).

The first portal with a 5-axis CNC unit has high stiffness and was built for machining with high precision. It has an integrated spindle for milling and sawing, but it can also perform other tasks, such as picking up different tools, holding a shield or temporary formwork for slip-forming, giving temporary support (e.g. in case of notches, window cut-outs, flat angles) or holding trowels for processing surfaces (e.g. increasing surface precision or decreasing surface roughness). The second portal carries an encapsulated robotic arm for heavy payloads of up to 150 kg. Due to its six degrees of freedom, the robotic arm supports a larger working space of 3.50 m × 7.70 m × 15.50 m (height × width × length). The robotic unit is designed to perform complex tasks with high motion dynamics, e.g. handling the spraying

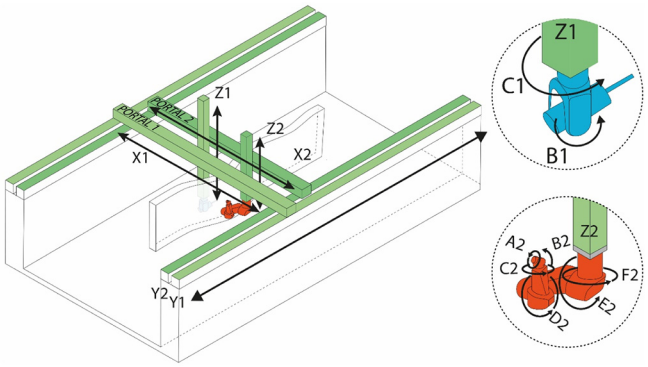

Fig. 1. Schematic illustration of the DBFL with its two digital units, which can work synchronously, cooperatively or independently working synergistically.

nozzle in case of SC3DP. By integrating the robotic arm with six degrees of freedom into a gantry with three axes, the advantages of high flexibility and high speed of the industrial robot, and the high range and rigidity of the portal system are combined synergistically. The system is controlled by a tailored software environment including a Sinumerik 840D (Siemens AG, Germany) controller as well as an individually tailored CAD tool for simulation and planning of processes.

2.2. SC3DP process setup

The development of the SC3DP technology required a specific process designed for the wet-mix concrete spraying process. Within the first stage of development presented here, the material is mixed in a horizontal pan-type mixer with high mixing energy (Mader, Germany) and filled into an electric screw pump (Variojet FU, Mader, Germany) with a conveyance capacity of 0.2–2.2 m^3/h. For standard operation, a rubber hose with a length of 20 m and an internal diameter of 35 mm is used. Pressure sensors at the beginning (Hygrosens DRTR-AL-20MA-R25B) and at the end of the conveyance line (Labom Compact CC6010) give an indication on the material behavior within the process (i.e., feeding problems and blockages). At the robot flange, the spraying nozzle (Repronozzle NW 15, Mader, Germany) is attached. At the nozzle, the material is accelerated by controlled addition of compressed air. Liquid chemical admixtures (e.g. set accelerators) can be injected into the compressed air stream by a dosing pump, which allows for a precise control of the amount of admixtures. Due to the high air pressure, the concrete is torn up in the nozzle, resulting in a high contact surface area between the concrete and the air stream, allowing for an appropriate intermixing of admixtures.

The three axes of the portal together with the 6-axes robot allow for a huge flexibility for manifold applications, which are illustrated exemplarily in Fig. 2. The SC3DP process generally allows for material deposition either in linear layers (Fig. 2, a), or with overlapping rotational movement (Fig. 2, b) as well as building-up elements with varying angles (Fig. 2, c). The layer thickness can be controlled by the robot speed (path velocity, Fig. 2, d), whereas the layer width can be adjusted by varying the nozzle distance from the surface (Fig. 2, e) [25,27]. In addition, the application process can be actively controlled by comparing the printed with the nominal values based on in-situ measurements of the applied layer geometry (distance and width) (Fig. 2, f). Moreover, the ability of synchronizing the measuring system with the position and the movement of the robot, helps facilitating adaptive fabrication. More details on the active process control are given in [24,27]. Due to the high flexibility of the process and the online process control, complex geometries (e.g. overhangs) as well as the integration of reinforcement or built-in parts can be realized [27–32].

One key challenge of process automation is to understand and redefine the entire concrete spraying process with all its interdependent

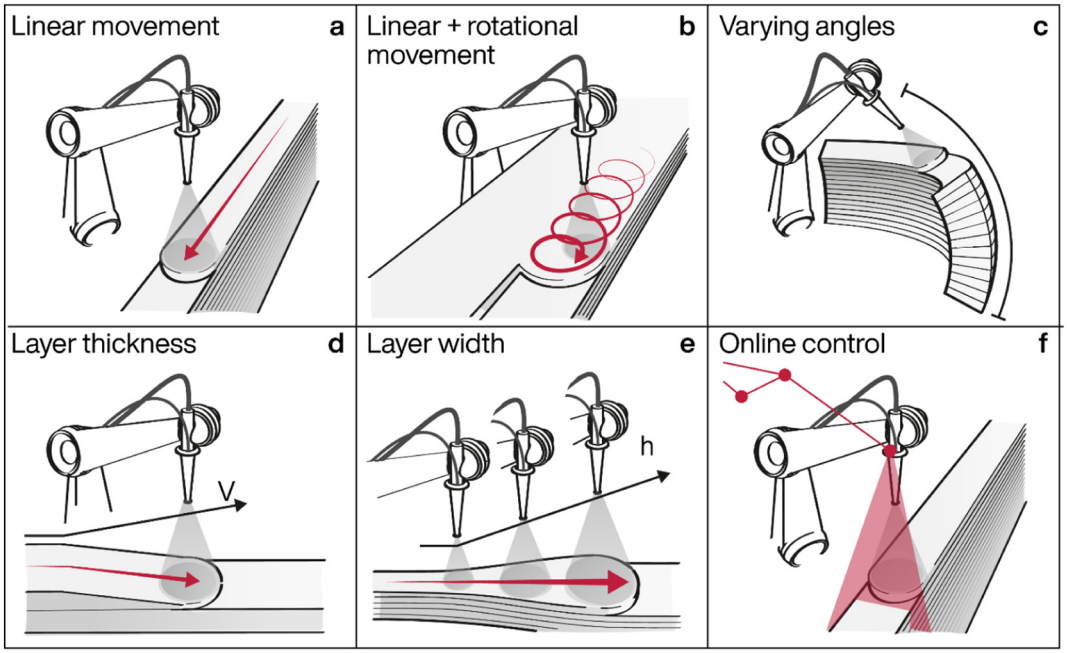

Fig. 2. Specific deposition methods of the SC3DP process: a) layer-by-layer deposition, b) laminar application, c) variation of application angle, d) control of layer thickness by robot speed (V), e) control of layer width by nozzle distance (h), and f) line laser for in-situ measurement of layer distance and width.

parameters. Therefore, the analysis of the shear rates and shear stresses, to which the material is exposed in the different processing steps (mixing, pumping, conveying, spraying), is crucial. With that knowledge, a precise and specific adjustment of material mix composition and of individual processing tools has to be carried out. More details on the individual aspects as well as first results on the process-material interactions are presented in [26,29].

3. Effect of process and material parameters on interlayer bond properties

3.1. Materials and mix proportions

For the present study, a commercially available spraying mortar (Nafufill KM 250, MC Bauchemie Müller, Bottrop, Germany) was used (Table 1). The binder phase consisted of Ordinary Portland cement (OPC, CEM I 52.5 R according to EN 197-1) and two different pozzolans. Quartz sand with a maximum grain size of 2 mm was used as aggregates. Moreover, the mixture contained the following pulverized chemical admixtures: shrinkage reducing agent (15 kg/m^3), chromate reducing agent (5 kg/m^3), re-dispersible polymer powder (5 kg/m^3), PCE superplasticizer (5 kg/m^3) and micro polypropylene fibers (3 kg/m^3). The equivalent water-to-cement ratio was 0.27. The mix composition was chemically and granulometrically optimized for dry shotcrete application, e.g. the dry components are constituted to dissolve or re-disperse within a short time after water addition during mixing. No accelerating admixtures were used in the present study, with the intent of providing a material with mainly rheology-dependent performance within the first two hours. Results on Shotcrete 3D Printing using accelerating admixtures are presented elsewhere [23].

Table 1
Mix proportions of the concrete used for 3D printing; all numbers have the unit kg/m^3.

OPC	Pozzolan	Silica fume	Sand	Water
500	160	25	1180	160

3.2. Material processing

The experiments were conducted at full scale (DBFL research facility) in order to cover all influencing factors from processing, particularly the material-process interactions. This is because simplified laboratory setups may not cover the effect of all processing steps (pumping pressure, hose length, hose curvatures, etc.) exactly, leading to differences in shear loads and hence to a different material performance during processing or after deposition. For comparison purposes, the same experimental program was carried out for both, Shotcrete 3D Printing and extrusion 3D printing.

The material was mixed in batches of 30–50 l and pumped to the end effector where it was applied either by spraying or by extrusion. For spraying, a rubber shotcrete nozzle with a length of 210 mm and an opening of 15 mm was used, whereas the extrusion nozzle had a rectangular opening of 20 mm × 25 mm. Simple wall-like specimens were built up layer-by-layer. Each specimen consisted of 10 layers with a total specimen height of about 200 mm (Fig. 3). The processing parameters (Table 2) were adjusted in order to achieve a layer height of approx. 20 mm by both printing methods. Due to the higher kinetic energy of the sprayed material and the larger diameter of the spray jet, the layers of SC3D printed specimens generally exhibit larger widths and slightly lower heights (Fig. 4). Linear specimens of 1000 mm length were SC3D printed, whereas squares with edge lengths of 400 mm were 3D printed by extrusion in order to achieve a good shape stability of the green specimens with regard to the reduced layer width. Due to the bidirectional (linear) material application in case of SC3DP, the standard time interval between the deposition of two layers varied between 1 and 20 s, whereas in case of extrusion the time interval was constant 24 s (Table 2).

To characterize the risk of cold joints formation, the specimens were produced in two steps as follows. The first five layers were produced continuously, i.e., the time lapse between the application of two subsequent layers resulted from the processing parameters. Then, the process was interrupted for different time intervals (delay times t_D): $t_{D,A}$ = 0 min, $t_{D,B}$ = 15 min, $t_{D,C}$ = 60 min and $t_{D,D}$ = 120 min. After the interruption, the layers no. 6–10 were produced. During the whole application process, the material properties were controlled by testing

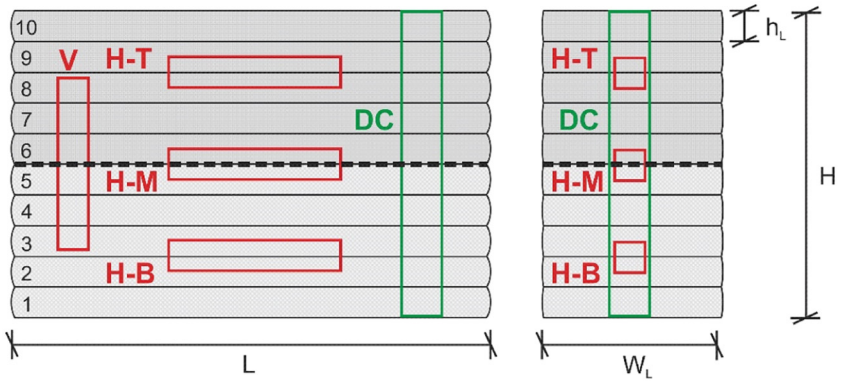

Fig. 3. Principle of sampling: longitudinal section (left) and cross section (right); prisms for mechanical testing were cut vertically (V) and horizontally (H) from the top (H-T), the middle (H-M) and the bottom (H-B) section; drilling cores (DC) were taken for CT scans; the main layer interface is marked by the dashed line.

Table 2
Processing parameters for both 3D printing methods used.

Parameter	SC3DP	Extrusion
Material mass flow (kg/h)	1829	1004
Air pressure at the nozzle (bar)	1.8–2.2	–
Compressed air volume (m^3/h)	55	–
Robot speed (mm/min)	6000	4000
Standard time interval between two layers (s)	1–20	24
Nozzle distance (mm)	200	0
Resulting layer height h_L, average (mm)	18.6	19.9
Standard deviation (mm)	1.46	1.64
Resulting layer width W_L (mm)	140–149	77–90

the following parameters: slump, slump loss, bulk density, air void content, temperature and penetration resistance.

The specimens were covered with plastic foil 2 h after production and stored at room temperature for 7 days. After 7 days, prisms for bending tests were cut from the main specimens following the principle shown in Fig. 3 and stored at 20 °C above water (100% rel. h.). The prisms had lengths of 120 mm and edge lengths of 25 mm. Every prism contained one layer interface allocated exactly at middle height, whereby it has to be distinguished between “normal” layer interfaces (deposition without interruption, i.e., layers no. 1–5 resp. 6–10) and the “main” layer interface between layers 5 and 6. Prisms were taken from the middle, top and bottom sections, denoted H-M, H-T and H-B, respectively (Fig. 3). Additional prisms (V) were taken vertically, with the “main” layer interface being allocated in the middle cross section. For referencing, standard prisms were prepared by casting the same material in moulds and vibrating (vibrated specimens).

3.3. Test methods

3.3.1. Testing of fresh concrete

Interlayer bond strength and other mechanical properties of 3D printed concrete elements are strongly influenced by structural build-up velocity of the material. Hence, the yield stress evolution of the material was characterized by penetration resistance tests to better interpret results of mechanical testing. Therefore, separate specimens consisting of three layers were produced by both 3D printing methods. The specimens had a length of approx. 1000 mm and different widths, depending on the 3D printing method (Section 3.2). The penetration resistance tests were conducted with a handheld shotcrete penetrometer (Mecmesin, UK) from 10 up to 180 min after mixing in the centre of the layers of 3D printed specimens. The penetrometer needle had a diameter of 3 mm, a cylindrical height of 12.5 mm and a cone height of 2.5 mm. From the measured normal force values, yield stresses were determined using the calculation approach for a conical tip connected with a cylinder rod as proposed by [33]. In contrast to [33], the loading speed was higher than 1 µm/s (manual handling of the penetrometer, “fast penetration test”). Hence, results give only approximations of the yield stress.

3.3.2. Mechanical testing of hardened concrete

Three-point bending tests and compressive strength tests were

Fig. 4. Specimen production within the DBFL by SC3DP (left) and extrusion 3D printing (right).

carried out on all sample categories at an age of 14 days. Additional strength tests on vibrated specimens at an age of 28 days revealed a minimal strength gain between 14 and 28 days (flexural strength: 7.5 vs. 7.4 N/mm^2, and compressive strength: 59.3 vs. 56.9 N/mm^2, resp.).

3.3.3. Computed tomography

From every main specimen two drilling cores were taken over full height and analyzed by computed tomography (CT) as follows. The cores were scanned with a GE phoenix|v tome|s cone X-ray CT device (GE Sensing & Inspection Technologies, Germany). Parameters for the CT scans were 150 kV tube voltage, 240 µA tube current, and 200 ms exposure time with a 0.1 mm Cu-filter. The scans had a voxel edge length of 36 µm. From the scans, the 3D structure was reconstructed with phoenix datos|x 2 (GE Sensing & Inspection Technologies, Germany) and converted to RAW-files with VGStudio 2 (Volume Graphics, Germany). The RAW-files were finally imported into Matlab 2017b (The Mathworks, US) and processed with a custom script. The script features automatic threshold segmentation of the air voids. The air void fraction was analyzed as a function of the vertical slice number. Hence, the air void content can be assessed in vertical slices along the full height in 36 µm increments. For each of the specimens more than 5500 slices were analyzed by the algorithm.

3.4. Results and discussions

3.4.1. Penetration resistance

The normal forces measured by penetration resistance tests and the calculated yield stresses are plotted over time in Fig. 5. The results reveal significant differences between SC3D printed and extruded samples. From the beginning, SC3D printed samples show a higher penetration resistance (resp. yield stress at approx. 10 kPa) as compared to extruded samples (approx. 6 kPa). In addition, after 70 min a steep increase was observed for SC3D printed samples.

One explanation for the generally higher level of yield stress could be the increase in bulk densities achieved by SC3DP (Section 3.4.2). As a consequence, smaller distances have to be bridged by the hydration products due to the reduced pore volume, resulting in earlier percolation and hence earlier structural build-up and setting [34–37]. For the yield stress increase of SC3D printed samples after 70 min no clear explanation can be given so far.

3.4.2. Bulk density, flexural and compressive strength

The results of bulk density and mechanical properties at an age of 14 days are summarized in Fig. 6. In case of printed specimens, mean values for all delay times investigated (t_D = 0, 15, 60 and 120 min) are given in the diagram. The coefficients of variation (CV's) of bulk density results are lower than 1.6% for all types of specimens and delay times. The CV's of compressive strength results are in the range of 5–8% (SC3DP) resp. 5–10% (extrusion), whereby no clear influence of t_D on CV was found. However, flexural strength results show significantly greater scattering in case of both printing methods. While SC3D printed specimens exhibit CV's from 9 to 18%, the CV's of extruded specimens are in the range of 12–44%. In case of both printing methods, there's a clear trend to an increased scattering of flexural strength results for higher delay times.

Noticeably, bulk densities of printed specimens are higher as compared to vibrated specimens, with SC3D printed samples showing the highest values (2.203 resp. 2.172 kg/dm^3), followed by extruded (approx. 2.055 kg/dm^3) and vibrated samples (2.019 kg/dm^3), Fig. 6. This may be attributed to the acceleration of the sprayed material due to the addition of compressed air, with its high kinetic energy leading to a better compaction of the substrate layer and of the layer interface region. Results also indicate that the extrusion process parameters used here enable proper material compaction.

The results show that both, the alignment of the main layer interface as well as the printing technique used, have a great influence on mechanical properties. When the main layer interface is aligned horizontally, i.e., perpendicularly to the load direction, SC3D printed samples show enhanced flexural and compressive strength compared to vibrated samples (SC3DP – H in Fig. 6). In contrast, extruded samples exhibit significantly lower flexural strength, but slightly increased compressive strength compared to vibrated specimens (Extrusion – H in Fig. 6). However, when the main layer interface is aligned parallel to the load direction (SC3DP and Extrusion – V in Fig. 6), all printed specimens show lower flexural strength, whereby the strength loss is more pronounced for extruded samples. On the other hand, the compressive strengths of printed samples are comparable to the vibrated samples or even higher (SC3DP).

To better understand the effect of bulk density variation on mechanical properties, the compressive strength and flexural strength results of all types of specimens (mean values, H-T, H-M and H-B are summarized as H, see also Fig. 3) are displayed over bulk density in Fig. 7. As can be seen, the compressive strength results are well correlated to bulk density, with SC3DP samples showing somewhat greater scattering than extruded or vibrated samples. The results confirm that there is little or no effect of interlayer bond strength on compressive strength, regardless of delay time. On the other hand, flexural strength results show significant scattering, indicating that results may be influenced by additional parameters or mechanisms than bulk density. Moreover, the prisms with the main layer interface being allocated normal to the prism axis (V) exhibit significantly lower flexural strength, indicating a clear effect of the interlayer bond strength of the main layer interface on flexural strength.

To investigate the effect of delay time t_D on interlayer bond properties, in Fig. 8 the flexural strength results are displayed over t_D differentiated according to the original height position and orientation of the prisms. Generally, no clear correlation between the height position of the prisms taken horizontally (H samples) and flexural strength can be observed. Surprisingly, for both 3D printing methods an increase in delay time has no significant effect on the flexural strength when the

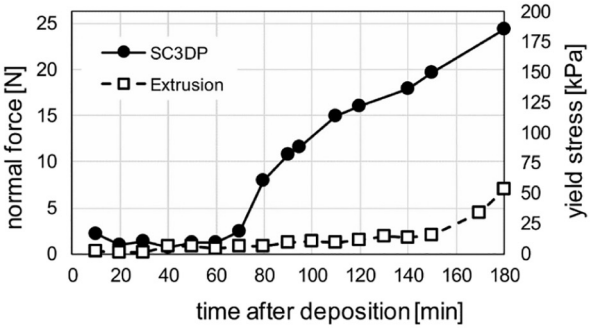

Time interval (min)	Yield stress (kPa)	
	SC3DP	Extrusion
15	11.9	2.2
60	9.9	4.6
120	122.6	11.4

Fig. 5. Normal force and yield stress over time for SC3D printed and extruded samples; yield stress values are given for the time intervals (delay times) 15, 60 and 120 min in the table (right).

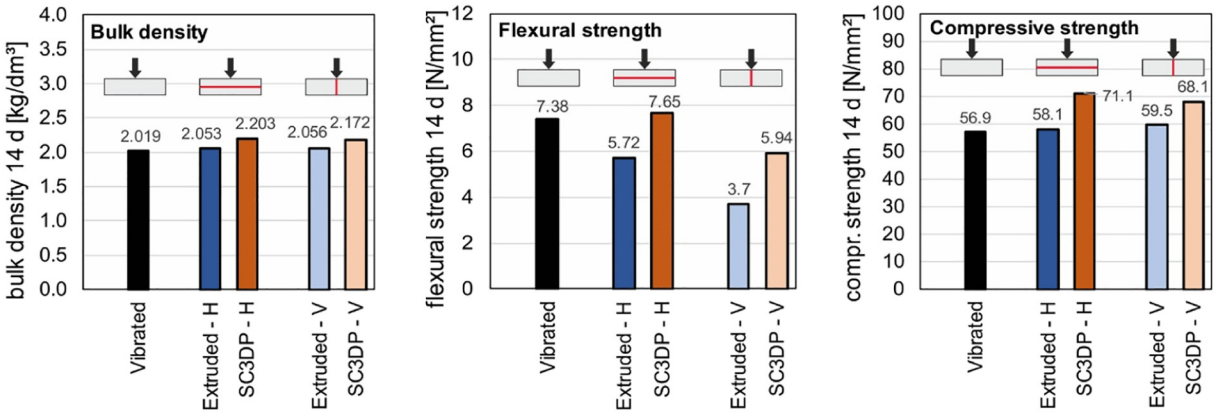

Fig. 6. Results of bulk density (left), flexural strength (centre) and compressive strength (right) of vibrated, SC3D printed and extruded specimens; H: horizontal layer alignment (main layer perpendicular to load direction), V: vertical layer alignment (main layer parallel to load direction); the values for horizontal alignment are mean values of all horizontally taken prisms (H-T, H-M, H-B, see also Fig. 3).

layer interfaces are allocated horizontally in the test (perpendicularly to the load direction, H samples).

In contrast, a clear effect of a prolonged delay time on flexural strength is evident when the main layer interface is aligned parallel to the load direction (V samples, Fig. 3). In case of SC3DP, flexural strength decreases when delay time is increased from 0 to 15 min, but for longer delay times no significant further strength reduction could be observed. However, in case of extrusion, longer delay times effect a greater loss of flexural strength, whereas for t_D = 15 min a relative strength increase was observed. So far, no clear explanation can be given for those exceptional results.

The results show that SC3D printed specimens exhibit excellent mechanical properties even in comparison to reference (vibrated) specimens. An increase in delay time between the deposition of two adjacent layers effects a significant reduction of interlayer bond strength. However, longer delay times (60 and 120 min) do not lead to further strength reduction. The results indicate that in case of SC3DP, process interruptions can be better tolerated without loss of mechanical performance. The excellent mechanical properties of SC3D printed specimens may be attributed to the improved compaction and the increased bulk density. Moreover, the improved mechanical interlocking between adjacent layers may play an important role (Section 3.4.3).

3.4.3. Air void volume and air void distribution from CT scans

For additional information on microstructural inhomogeneities or anisotropies as an explanation of the mechanical performance, air void distributions within the specimen volume (example in Fig. 9) and mean values of air void content for different time intervals t_D (Fig. 10) were assessed by CT scans. A characteristic difference was found in the air void contents between extruded and SC3D printed samples, corresponding to the differences in bulk density. The extruded specimens show significantly higher mean values of air void content at 3.4% (average of all values for extrusion given in Fig. 10), which is likely attributed to the lower kinetic energy of the extruded material, and hence, a lower compaction as compared to the sprayed material (mean values of air void content of approx. 1.5%).

Moreover, for extruded specimens the average air void content increases with delay time whereas no clear effect of t_D could be identified for SC3D printed specimens (Fig. 10). However, both types of specimens show considerable microstructural inhomogeneities, i.e., sharp minima or maxima of the air void content in the vicinity of the layer interfaces. This is confirmed by the greyscale and false color images in Fig. 9. Extruded specimens porosities are higher in the top section of the lower layer (zone 1) as compared to SC3D printed specimens (Fig. 9, d and e vs. h and i), whereas porosity is increased in the bottom section of the upper layer (zone 2) in case of both processes (Fig. 9, b and c vs. f and g). Both types of specimens show marked differences (jumps) between minimum porosity (zone 1) and maximum porosity (zone 2) at each layer interface, with the SC3DP samples showing pronounced maxima and minima, whereas in case of extruded samples the minima are more pronounced than the maxima.

The pronounced porosity maximum in the upper boundary of the printed samples could be explained by an inclusion of air bubbles, which is slightly more pronounced for SC3DP. This may be due to the higher application speed (path velocity), the spray jet velocity and the high viscosity of the sprayed material. However, the effect of those microstructural inhomogeneities on strength is lower than expected in case of SC3DP (Section 3.4.2). This may be attributed to greater

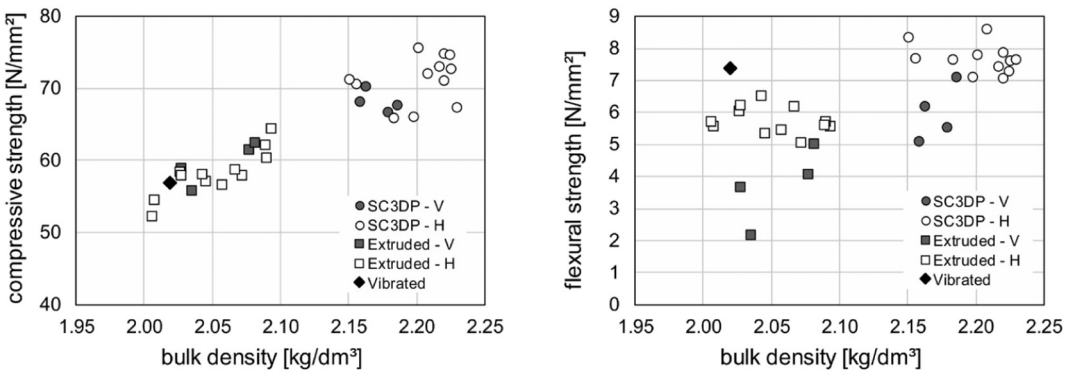

Fig. 7. Compressive strength (left) and flexural strength results (right) of SC3D printed, extruded and vibrated samples at an age of 14 days for all delay times t_D; prisms taken vertically (V) and horizontally (H) from the main specimen, with the layer interfaces allocated normal (V) or parallel (H) to the prism axis.

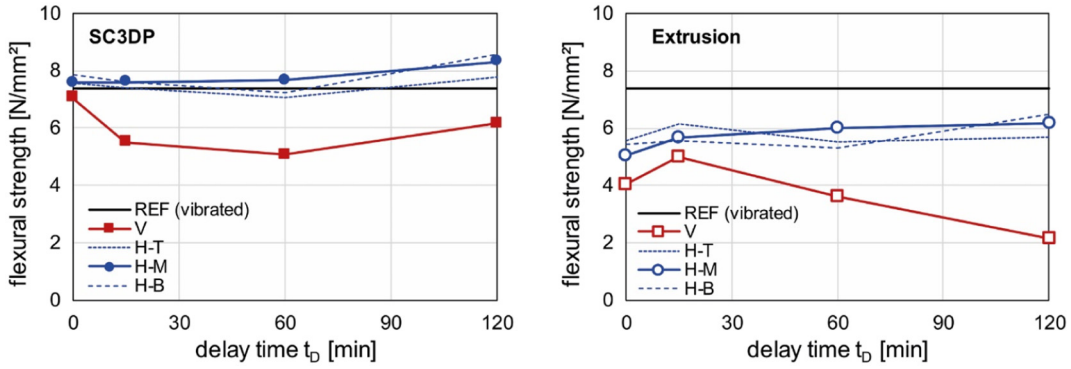

Fig. 8. Flexural strengths of SC3D printed, extruded and vibrated samples at an age of 14 days over delay time; prisms were cut from the main specimens vertically (V) and horizontally (H-T, H-M, H-B), with the main interface allocated normal (V) or parallel (H-M) to the prism axis (see Fig. 3).

compaction of the sprayed material, which is to a high degree caused by the high kinetic energy of the sand grains. On the other hand, a small amount of rebound of the larger grains must always be taken into account, while the main share of the grains penetrates the lower layer, hence possibly creating a pronounced macroscopic roughness of the layer interface.

In case of extrusion, the porosity deviation from the median value is higher as compared to SC3DP (standard deviation SD of 1.02% vs. 0.64%, coefficient of variation CV of 30% vs. 44%). The higher SD values could partially explain the poorer mechanical performance of extruded samples, as they represent the absolute differences in porosity over sample height. As can be seen from the CV results, the relative differences in porosity over height are greater in case of SC3DP. However, this effect seems to have a lower impact on mechanical

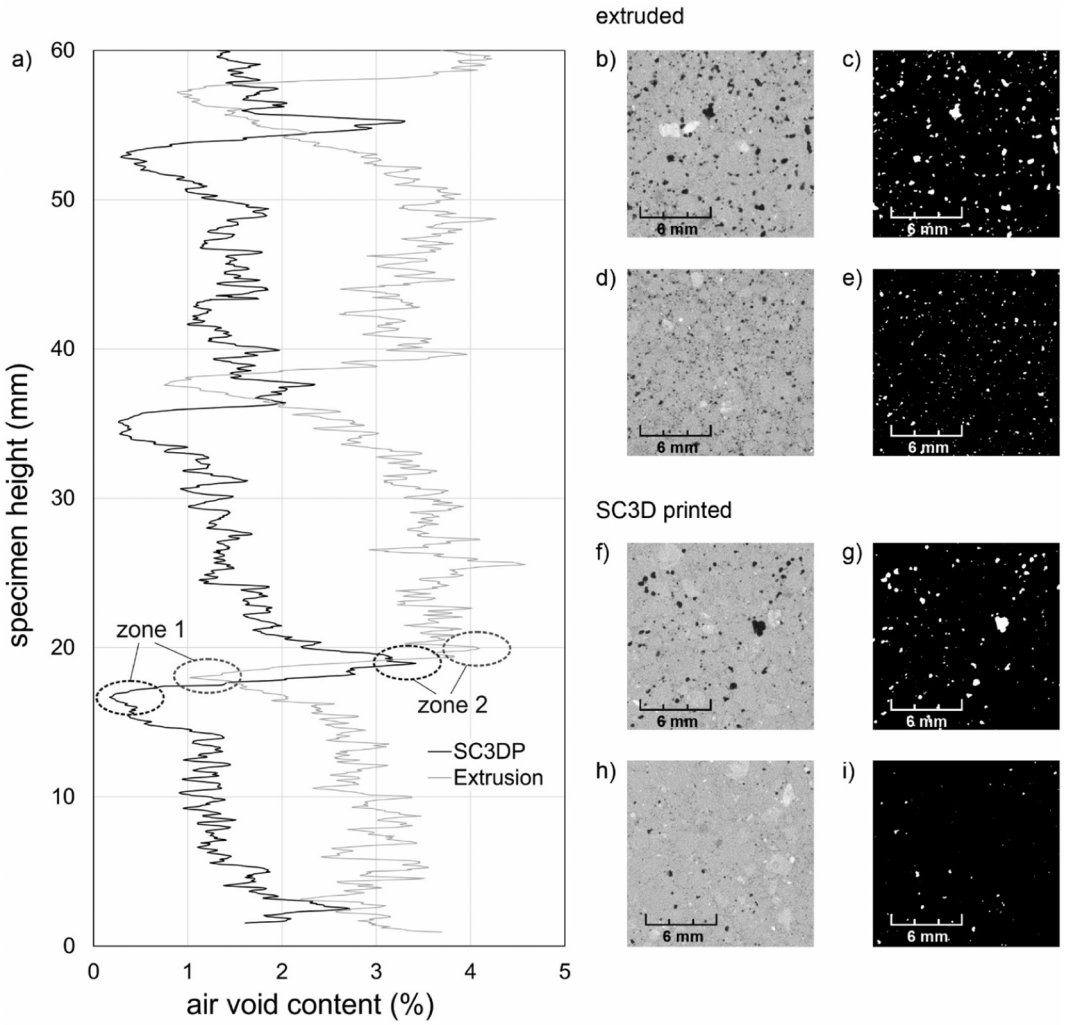

Fig. 9. Air void content of 3D printed specimens without process interruption along the specimen height (a) and CT scan images of extruded (b–e) and SC3D printed specimens (f–i); images b, c and f, g show the lower region of the upper layer (zone 1), images d, e and h, I the upper region of the lower layer (zone 2). The false color images (c, e, g, i) display the results of the air void determining algorithm.

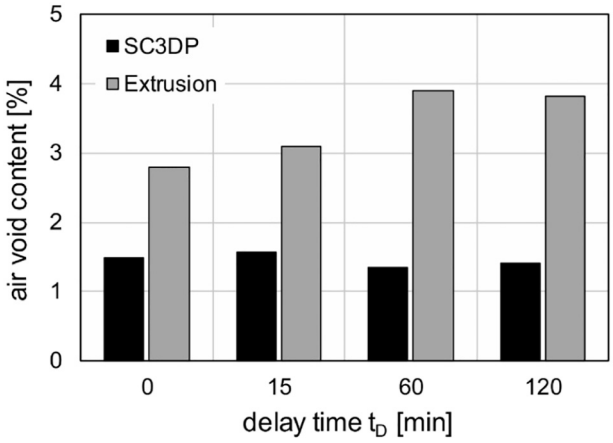

Fig. 10. Mean values of air void content over full sample height for different time intervals (delay times) t_D.

performance than the absolute differences (SD). Moreover, the average air void content of extruded specimens slightly increases with t_D, which was not observed in case of SC3DP (Fig. 10). The porosity peak in zone 2 for both printing methods may be explained by air void inclusions, whereas the pronounced porosity minimum in zone 1 indicates a compaction effect by horizontal movement of the extruder head.

Additional information on the macroscopic roughness of the main layer interface was gathered by producing specimens with barite ($BaSO_4$) spread on each deposited layer before the next layer was applied. Barite has a greater X-ray attenuation than cementitious material. Accordingly, it can be easily detected in the CT data [38]. Cylinders with radii of 15 mm were extracted by core drilling and subsequently CT scanned.

The CT slices show a different barite distribution in the interface zones of samples produced by extrusion and by SC3DP, respectively (Fig. 11). Clearly, SC3D printed samples show a much higher interface roughness, resulting in enhanced interlocking and an increased adhesion due to the higher specific interface surface. In contrast, extruded samples exhibit a smooth interface. Due to the specific material deposition and distribution of the extrusion head by horizontal sliding, a slight compaction and levelling of the surface of the extruded layer is achieved, possibly resulting in weaker bond strength.

Those findings are in accordance with the statements in [20] with regard to the mechanisms determining shear and tensile bond strength. The effect of the increased surface roughness seems to be dominant compared to the faster structural build-up (i.e., increase in yield stress, Section 3.4.1), which after the state-of-knowledge should result in poorer interface bond strength [5,35,39]. For a quantitative assessment of the critical delay time for the deposition of subsequent material layers without the risk of cold joints formation with regard to the structural build-up, more investigations of the underlying mechanisms are required. Moreover, the effect of accelerating admixtures on both, the mechanical performance and the critical delay time has to be investigated in more detail. First results on the effect of accelerating admixtures on interlayer bond properties are presented in [23] for SC3D printing.

4. Conclusions

This paper presents the basic principles, process design and potentials of Shotcrete 3D Printing (SC3DP), especially with respect to interlayer bond strength. The technological capabilities of SC3DP are demonstrated by means of experimental studies on the mechanical and microstructural properties and compared to extrusion-based 3D printing. The results of the study presented here can be summarized as follows:

- SC3D printed samples show higher bulk densities as compared to extruded or vibrated samples, which is mainly caused by the enhanced material compaction due to the high kinetic energy of the sprayed material.
- The higher bulk densities of SC3D printed specimens result in increased compressive and flexural strengths as compared to extruded specimens, resp. in increased compressive strengths and comparable flexural strengths as compared to vibrated specimens.
- The delay time (varied between 0 and 120 min) had no significant effect on compressive and flexural strength in case of both printing methods when the main interface was aligned normally to the load direction.
- In case of the main interface aligned centrally and parallelly to the load direction, a negative effect of the layer interfaces and of increased delay times was observed, being more pronounced for extruded than for SC3D printed specimens. SC3D printed specimens were found to be less susceptible for loss of mechanical performance in case of process interruptions.
- As demonstrated by the air void content distribution over the layer height and within the interface zone from CT scan analysis, the excellent mechanical performance of SC3D printed specimens can be mainly attributed to enhanced interlocking (macro roughness) of the layer interface.

SC3DP technology, integrated into a robot-guided manufacturing environment, offers the potential to overcome current limitations in concrete 3D printing, such as reducing the risk of cold joint formation. Moreover, due to the high degree of geometric freedom, SC3DP allows for highly complex tasks, such as integration of reinforcement and surface finishing.

CRediT authorship contribution statement

Harald Kloft: Conceptualization, Funding acqusition, Methodology, Project administration, Resources, Visualization, Writing - original draft, Writing - review & editing. **Hans-Werner Krauss:** Conceptualization, Data curation, Investigation, Methodology, Validation, Visualization, Writing - original draft, Writing - review & editing. **Norman Hack:** Methodology, Writing - review & editing. **Eric Herrmann:** Conceptualization, Investigation, Visualization, Writing - original draft, Writing - review & editing. **Stefan Neudecker:** Funding acquisition, Writing - original draft. **Patrick A. Varady:** Data curation.

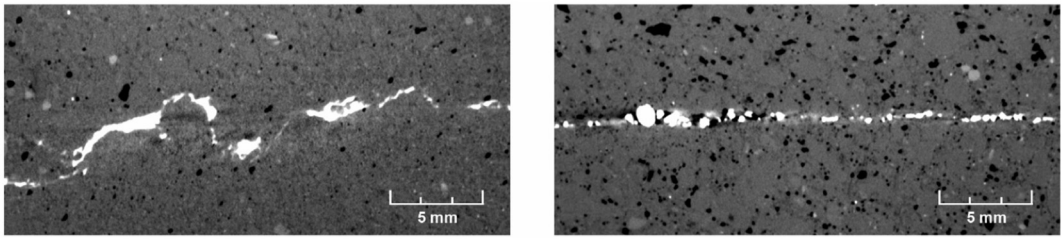

Fig. 11. CT slice of the barite (white areas) distribution in the contact zone between two layers (left: SC3DP, right: extrusion).

Dirk Lowke: Conceptualization, Methodology, Resources, Validation.

Declaration of competing interest

The authors declare that they have no known competing financial interests or personal relationships that could have appeared to influence the work reported in this paper.

Acknowledgements

The authors gratefully acknowledge the funding by the German Research Foundation (funded by the Deutsche Forschungsgemeinschaft (DFG), Project No 257311925 and 414265976) and the Ministry for Science and Culture of Lower Saxony. We also thank the company MC Bauchemie-Müller GmbH & Co. KG, Bottrop, Germany, for supplying the raw materials.

References

[1] C. Beyer, Strategic implications of current trends in Additive Manufacturing, J. Manuf. Sci. 136 (2014) 064701/1–8, https://doi.org/10.1115/1.4028599.
[2] N. Labonnote, A. Rønnquist, B. Manum, P. Rüther, Additive construction: state-of-the-art, challenges and opportunities - a review, Autom. Constr. 72 (2016) 347–366, https://doi.org/10.1016/j.autcon.2016.08.026.
[3] I. Agusti-Juan, F. Müller, N. Hack, T. Wangler, G. Habert, Potential benefits of digital fabrication for complex structures: environmental assessment of a robotically fabricated concrete wall, J. Clean. Prod. 154 (2017) 330–340, https://doi.org/10.1016/j.jclepro.2017.04.002.
[4] R.A. Buswell, W.R. Leal da Silva, F.P. Bos, R. Schipper, D. Lowke, N. Hack, H. Kloft, V. Mechtcherine, T. Wangler, N. Roussel, A process classification framework for defining and describing Digital Fabrication with Concrete, Cem. Concr. Res. (2020) accepted for publication.
[5] T. Wangler, E. Lloret, L. Reiter, N. Hack, F. Gramazio, M. Kohler, M. Bernhard, B. Dillenburger, J. Buchli, N. Roussel, R.J. Flatt, Digital concrete: opportunities and challenges, RILEM Tech. Lett. 1 (2016) 67–75, https://doi.org/10.21809/rilemtechlett.2016.16.
[6] R.A. Buswell, W.R. Leal de Silva, S.Z. Jones, J. Dirrenberger, 3D printing using concrete extrusion: a roadmap for research, Cem. Concr. Res. 112 (2018) 37–49, https://doi.org/10.1016/j.cemconres. 2018.05.006.
[7] V.N. Nerella, M. Krause, M. Näther, V. Mechtcherine, V, Studying printability of fresh concrete for formwork free concrete on-site 3D Printing technology (CONPrint3D), in: M. Greim, et al. (Ed.), Rheological Measurements on Construction Materials, Proceedings, Regensburg, 2016.
[8] V.N. Nerella, S. Hempel, V. Mechtcherine, Micro- and macroscopic investigations on the interface between layers of 3D-printed cementitious elements, in: M. Santhanam, et al. (Ed.), ICACMS 2017, Int. Conf. Adv. Constr. Mat. Syst., Chennai, India. RILEM Proceedings Pro 118, 2017, pp. 557–565.
[9] V.N. Nerella, S. Hempel, V. Mechtcherine, Effects of layer-interface properties on mechanical performance of concrete elements produced by extrusion-based 3D-printing, Constr. Build. Mater. 205 (2019) 586–601, https://doi.org/10.1016/j.conbuildmat.2019.01.235.
[10] S.C. Paul, Y.W.D. Tay, B. Panda, M.J. Tan, Fresh and hardened properties of 3D printable cementitious materials for building and construction, Arch. Civ. Mech. Eng. 18 (2018) 311–319, https://doi.org/10.1016/j.acme.2017.02.008.
[11] B. Zareiyan, B. Khoshnevis, Interlayer adhesion and strength of structures in Contour Crafting–effects of aggregate size, extrusion rate, and layer thickness, Autom. Constr. 81 (2017) 112–121, https://doi.org/10.1016/j.autcon.2017.06.013.
[12] B. Zareiyan, B. Khoshnevis, Effects of interlocking on interlayer adhesion and strength of structures in 3D printing of concrete, Autom. Constr. 83 (2017) 212–221, https://doi.org/10.1016/j.autcon.2017.08.019.
[13] T.T. Le, S.A. Austin, S. Lim, R.A. Buswell, R. Law, A.G.F. Gibb, T. Thorpe, Hardened properties of high-performance printing concrete, Cem. Concr. Res. 42 (2012) 558–566, https://doi.org/10.1016/j.cemconres.2011.12.003.
[14] P. Feng, X. Meng, J.F. Chen, L. Ye, Mechanical properties of structures 3D printed with cementitious powders, Constr. Build. Mater. 93 (2015) 486–497, https://doi.org/10.1016/j.conbuildmat. 2015.05.132.
[15] E. Hosseini, M. Zakertabrizi, A.H. Korayem, G. Xu, A novel method to enhance the interlayer bonding of 3D printing concrete: an experimental and computational investigation, Cem. Concr. Compos. 99 (2019) 112–119, https://doi.org/10.1016/j.cemconcomp.2019.03.008.
[16] T. Marchment, J.G. Sanjayan, B. Nematollahi, M. Xia, Interlayer strength of 3D printed concrete, in: J.G. Sanjayan, et al. (Ed.), 3D Concrete Printing Technology, Elsevier, 2019, pp. 241–264, , https://doi.org/10.1016/B978-0-12-815481-6.00012-9.
[17] R.J.M. Wolfs, F.P. Bos, T.A.M. Salet, Hardened properties of 3D printed concrete: the influence of process parameters on interlayer adhesion, Cem. Concr. Res. 119 (2019) 132–140, https://doi.org/10.1016/j.cemconres.2019.02.017.
[18] J.G. Sanjayan, B. Nematollahi, M. Xia, T. Marchment, Effect of surface moisture on inter-layer strength of 3D printed concrete, Constr. Build. Mat. 172 (2018) 468–475, https://doi.org/10.1016/j.conbuildmat. 2018.03.232.
[19] T. Wangler, N. Roussel, F.P. Bos, T.A.M. Salet, R.J. Flatt, Digital concrete: a review, Cem. Concr. Res. 123 (2019) 105780, , https://doi.org/10.1016/j.cemconres.2019.105780.
[20] H. Beushausen, M.G. Alexander, Bond strength development between concretes of different ages, Mag. Concr. Res. 60 (2008) 65–74, https://doi.org/10.1680/macr.2007.00108.
[21] C. Talbot, M. Pigeon, D. Beaupré, D.R. Morgan, Influence of surface preparation on long-term bonding of shotcrete, ACI Mater. J. 91 (1995) 560–566, https://doi.org/10.14359/1376.
[22] J. van der Putten, G. de Schutter, K. van Tittelboom, The effect of print parameters on the (micro) structure of 3D printed cementitious materials, in: T. Wangler, R.J. Flatt (Eds.), First RILEM International Conference on Concrete and Digital Fabrication–Digital Concrete 2018, Springer, 2019, , https://doi.org/10.1007/978-3-319-99519-9_22.
[23] I. Dressler, N. Freund, D. Lowke, The effect of accelerator dosage on fresh concrete properties and on interlayer strength in Shotcrete 3D Printing, Materials 13 (2020) 374, https://doi.org/10.3390/ma13020374.
[24] S. Neudecker, C. Bruns, R. Gerbers, J. Heyn, F. Dietrich, K. Dröder, A. Raatz, H. Kloft, A new robotic spray technology for generative manufacturing of complex concrete structures without formwork, Procedia CIRP 43 (2016) 333–338, https://doi.org/10.1016/j.procir.2016.02.107.
[25] E. Herrmann, H. Lindemann, H. Kloft, Development of a robotic sprayed concrete technology for generative manufacturing of complex concrete structures without formwork, in: W. Kusterle (Ed.), Spritzbeton-Tagung 2018, Proc., Alpbach, Austria, 2018 (in German).
[26] H.W. Krauss, N. Nolte, H. Budelmann, H. Kloft, D. Lowke, Additive Manufacturing with concrete – challenges and solutions illustrated by the SC3DP process, in: H.M. Ludwig, H.B. Fischer (Eds.), 20. Internationale Baustofftagung (Ibausil 2018), Proc., Weimar, 2018 9 pp. (in German).
[27] H. Lindemann, R. Gerbers, S. Ibrahim, E. Herrmann, F. Dietrich, K. Dröder, A. Raatz, H. Kloft, Development of a Shotcrete 3D Printing (SC3DP) technology for Additive Manufacturing of reinforced freeform concrete structures, in: T. Wangler, R.J. Flatt (Eds.), First RILEM International Conference on Concrete and Digital Fabrication–Digital Concrete 2018, Springer, 2019, , https://doi.org/10.1007/978-3-319-99519-9_27.
[28] H. Kloft, N. Hack, J. Mainka, L. Brohmann, E. Herrmann, L. Ledderose, D. Lowke, Additive Fertigung im Bauwesen: erste 3-D-gedruckte und bewehrte Betonbauteile im Shotcrete-3-D-Printing-Verfahren (SC3DP), Bautechnik 96 (2019) 929–938, https://doi.org/10.1002/bate.201900094 (in German).
[29] N. Nolte, M. Heidmann-Ruhz, H.-W. Krauss, P. Varady, H. Budelmann, A. Wolter, Development of shotcrete mixtures with controllable properties for the additive manufacturing of concrete structures, in: W. Kusterle (Ed.), Spritzbeton-Tagung 2018, Proc., Alpbach, Austria, 2018 (in German).
[30] H. Kloft, D. Lowke, N. Hack, 3D printing – an innovative an efficient technology for 3D printing of large-scale concrete components, Drymix Mortar Yearbook 3D Special, München, 2019, pp. 38–43.
[31] H. Kloft, N. Hack, J. Mainka, D. Lowke, Large Scale 3D Concrete Printing: Basic Principles of 3D Concrete Printing, CPT Worldwide, 2019, pp. 28–35.
[32] H. Kloft, M. Empelmann, V. Oettel, L. Ledderose, Production of the first concrete and reinforced concrete columns by means of 3D printing with concrete, BFT International: Betonwerk + Fertigteil-Technik 85 (2019) 28–37.
[33] D. Lootens, P. Jousset, L. Martinie, N. Roussel, R.J. Flatt, Yield stress during setting of cement pastes from penetration tests, Cem. Concr. Res. 39 (2009) 401–408, https://doi.org/10.1016/j.cemconres. 2009.01.012.
[34] N. Roussel, G. Ovarlez, S. Garrault, C. Brumaud, The origins of thixotropy of fresh cement pastes, Cem. Concr. Res. 42 (2012) 148–157, https://doi.org/10.1016/j.cemconres.2011.09.004.
[35] A. Perrot, D. Rangeard, A. Pierre, Structural built-up of cement-based materials used for 3D-printing extrusion techniques, Mater. Struct. 49 (2016) 1213–1220, https://doi.org/10.1617/s11527-015-0571-0.
[36] D. Lowke, Thixotropy of SCC-A model describing the effect of particle packing and superplasticizer adsorption on thixotropic structural build-up of the mortar phase based on interparticle interactions, Cem. Concr. Res. 104 (2018) 94–104, https://doi.org/10.1016/j.cemconres.2017.11.004.
[37] A. Perrot, D. Rangeard, E. Courteille, 3D printing of earth-based materials: processing aspects, Constr. Build. Mat. 172 (2018) 670–676, https://doi.org/10.1016/j.conbuildmat.2018.04.017.
[38] P. Carrara, R. Kruse, D.P. Bentz, M. Lunardelli, T. Leusmann, P. Varady, L. De Lorenzis, Improved mesoscale segmentation of concrete from 3D X-ray images using contrast enhancers, Cem. Concr. Compos. 93 (2018) 30–42, https://doi.org/10.1016/j.cemconcomp.2018.06.014.
[39] N. Roussel, F. Cussigh, Distinct-layer casting of SCC: the mechanical consequences of thixotropy, Cem. Concr. Res. 38 (2008) 624–632, https://doi.org/10.1016/j.cemconres.2007.09.023.